

Inhibiting radiative recombination rate to enhance quantum yields in a quantum photocell

Jing-Yi Chen(陈镜伊), Shun-Cai Zhao(赵顺才)

Citation: Chin. Phys. B . 2020, 29(6): 064207 . **doi:** 10.1088/1674-1056/ab836f
Journal homepage: http://cpb.iphy.ac.cn; http://iopscience.iop.org/cpb

What follows is a list of articles you may be interested in

Electromagnetically induced transparency and electromagnetically induced absorption in Y-type system

Kalan Mal, Khairul Islam, Suman Mondal, Dipankar Bhattacharyya, Amitava Bandyopadhyay

Chin. Phys. B . 2020, 29(5): 054211 . **doi:** 10.1088/1674-1056/ab7ea0

Dynamic manipulation of probe pulse and coherent generation of beating signals based on tunneling-induced inference in triangular quantum dot molecules

Nuo Ba(巴诺), Jin-You Fei(费金友), Dong-Fei Li(李东飞), Xin Zhong(钟鑫), Dan Wang(王丹), Lei Wang(王磊), Hai-Hua Wang(王海华), Qian-Qian Bao(鲍倩倩)

Chin. Phys. B . 2020, 29(3): 034204 . **doi:** 10.1088/1674-1056/ab683d

Interlayer distance effects on absorption coefficient and refraction index change in p-type double-*δ*-doped GaAs quantum wells

H Noverola-Gamas, L M Gaggero-Sager, O Oubram

Chin. Phys. B . 2019, 28(12): 124207 . **doi:** 10.1088/1674-1056/ab5278

All-optical switch and transistor based on coherent light-controlled single two-level atom coupling with two nanowires

Xin-Qin Zhang(张新琴), Xiu-Wen Xia(夏秀文), Jing-Ping Xu(许静平), Mu-Tian Cheng(程木田), Ya-Ping Yang(羊亚平)

Chin. Phys. B . 2019, 28(11): 114207 . **doi:** 10.1088/1674-1056/ab48f2

Dynamic and inner-dressing control of four-wave mixing in periodically-driven atomic system

Yuan-Yuan Li(李院院), Li Li(李莉), Yun-Zhe Zhang(张云哲), Lei Zhang(张雷)

Chin. Phys. B . 2019, 28(10): 104201 . **doi:** 10.1088/1674-1056/ab3b52

Inhibiting radiative recombination rate to enhance quantum yields in a quantum photocell*

Jing-Yi Chen(陈镜伊) and Shun-Cai Zhao(赵顺才)†

Department of Physics, Faculty of Science, Kunming University of Science and Technology, Kunming 650500, *China*

(Received 29 December 2019; revised manuscript received 24 February 2020; accepted manuscript online 26 March 2020)

Inhibiting the radiative radiation is an efficient approach to enhance quantum yields in a solar sell. This work carries out the inhibition of radiative recombination rate (RRR) in a quantum photocell with two coupled donors. We perform explicit calculations of the transition rates, energy gaps and the absorbed solar wavelength-dependent RRR, and find that two different regimes play the crucial roles in inhibiting RRR. One is the quantum coherence generated from two different transition channels, the other includes the absorbed photon wavelength and gaps between the donor and acceptor in this proposed photocell model. The results imply that there may be some efficient ways to enhance the photoelectron conversion compared to the classic solar cell.

Keywords: radiation recombination rate, photoelectric conversion efficiency, quantum photocell

PACS: 42.50.Gy **DOI:** 10.1088/1674-1056/ab836f

1. Introduction

The photoelectron conversion efficiency[1–4] is a continuous concern about solar cells or photovoltaic devices. When research of the photoelectric conversion efficiency encounters the bottleneck,[5–14] scientists turn their interesting to quantum technology,[15–25] and they hoped to break through the efficiency limitation, and further to improve the photoelectric conversion efficiency by means of quantum mechanics.

When it comes to efficiency losses, there are two categories efficiency loss processes in the photovoltaic devices. One is the extrinsic losses such as series resistance,[26–28] parasitic recombination and contact shadowing,[29] they are theoretically avoidable and consequently are not considered in fundamental limiting efficiency. The other is the intrinsic losses such as non-absorption of photons with energy below the bandgap,[30–32] thermalisation loss[33–35,37] due to strong interaction between excited carriers and lattice phonons and emission loss according to Kirchoff's law,[37,38] they are unavoidable in device design and will still be present in an idealized solar cell.[6] What is more, the radiative upward transition and its reversal, the radiative downward transition coexist simultaneously,[39] which has been considered as the fundamental limit[5] on the conversion efficiency. Scully[15] proposed a scheme to reduce radiative recombination via the quantum coherence with or without the drive field. Svidzinsky *et al.*[17] manifested that quantum coherence could increase the flow of electrons through the load and enhance cell power via the reduction of radiative recombination. Creatore *et al.* showed that quantum interference induced by the dipole-dipole interaction between molecular excited states guarantees an enhanced light-to-current conversion and power.[40]

In this paper, we explicitly consider the regulation mechanism of radiative recombination rate (RRR) in a quantum photocell with two coupled donors, and this intention requires a more detailed density matrix analysis via the master equations for this quantum open system. Furthermore, we focus on the inhibited RRR by quantum coherence generated from two different transition channels and by other controlled parameters of this photocell system. As compared to Ref. [15], some more explicit principal issues rather than practical implications are discussed deeply.

2. The photocell model with two electron donors

Before explicitly visiting the performance of quantum photocell (seen in Fig. 1), we describe the quantum photocell model firstly. The introduced photocell consists of the conduction band states $|a_i\rangle_{(i=1,2)}$ and valence band state $|b\rangle$ as the donor, level $|c\rangle$ and level $|v\rangle$ as the acceptor connected to the external circuit. The two conduction band states $|a_i\rangle_{(i=1,2)}$ and the ground state $|b\rangle$ are modeled as two dipole-dipole coupled donors, which is similar to the model of Creatore *et al.*[40] The optical transition in coupling of two conduction band states $|a_i\rangle_{(i=1,2)}$ and valence band state $|b\rangle$ is characterized by the optical dipole moment $\boldsymbol{\mu} = e\langle b|\boldsymbol{r}|a\rangle$. As for the intermolecular interaction in a molecular aggregate, which is composed of two electric neutral molecules, can be described by the electrostatic dipole–dipole coupling[41]

$$J_{12} = \frac{1}{4\pi\varepsilon\varepsilon_0}\left(\frac{\boldsymbol{\mu}_{a_1}\cdot\boldsymbol{\mu}_{a_2}}{r^3} - \frac{3(\boldsymbol{\mu}_{a_1}\cdot\boldsymbol{r})(\boldsymbol{\mu}_{a_2}\cdot\boldsymbol{r})}{r^5}\right), \quad (1)$$

*Project supported by the National Natural Science Foundation of China (Grant Nos. 61565008 and 61205205) and the General Program of Yunnan Applied Basic Research Project, China (Grant No. 2016FB009).

†Corresponding author. E-mail: zhaosc@kust.edu.cn

© 2020 Chinese Physical Society and IOP Publishing Ltd

where the dipole moments $\boldsymbol{\mu}_{a_1}$ and $\boldsymbol{\mu}_{a_2}$ are located at $\boldsymbol{r}_{a_1}$ and $\boldsymbol{r}_{a_2}$, respectively; and $\boldsymbol{r} = \boldsymbol{r}_{a_1} - \boldsymbol{r}_{a_2}$ is the radius vector from $\boldsymbol{r}_{a_1}$ to $\boldsymbol{r}_{a_2}$. For simplicity, we assume that the two donors are identical and degenerate, so two coupled excited states $|a_1\rangle$ and $|a_2\rangle$ of the two donors have the same excitation levels $E_{a1} = E_{a2} = \hbar\omega$. Furthermore, their dipole moments are aligned in the same direction, $\boldsymbol{\mu}_{a_1} = \boldsymbol{\mu}_{a_2} = \boldsymbol{\mu}$ as depicted in Fig. 1. The Hamiltonian for the system of two interacting donors reads

$$\hat{H} = \sum_{i=1,2} \hbar\hat{\omega}_i \hat{\sigma}_i^{\dagger} \hat{\sigma}_i^{-} + J_{12}(\hat{\sigma}_1^{-}\hat{\sigma}_2^{\dagger} + \hat{\sigma}_2^{-}\hat{\sigma}_1^{\dagger}), \tag{2}$$

where $\hat{\sigma}_{i(i=1,2)}^{\dagger} = |a_i\rangle\langle b|$ and $\hat{\sigma}_{i(i=1,2)}^{-} = |b\rangle\langle a_i|_{i=1,2}$ are the Pauli rising and falling operators, respectively. Generally speaking, the coupling strength J_{12} is weaker than excitation energy $\hbar\omega = E_a - E_b$ with $E_a = E_{ai,(i=1,2)} + \sqrt{2}J_{12}$.[40] The cycle procedure starts in the ground state $|b\rangle$ absorbing solar photons. The electron transport begins with the population on the two coupled donor excited states $|a_i\rangle_{(i=1,2)}$. Next, the excited electrons are transferred to the acceptor molecule, the charge-separated state $|c\rangle$. In the quantum heat engine describing of a solar cell,[42] the acceptor's states $|c\rangle$ and $|v\rangle$ represent the conduction and the valence band, respectively. The excited electron is then assumed to be used to perform work, leaving the charge-separated state $|c\rangle$ decaying to the sub-stable state $|v\rangle$, and the resistance of an external load connected to them is characterized by the decay rate Γ of electrons from $|c\rangle$ to $|v\rangle$. The electronic current flowing from the conduction band state $|c\rangle$ to the valence band state $|v\rangle$ is given by $j = e\Gamma p_c$, where e and p_c represent the fundamental charge of an electron and conduction band population, respectively. The voltage across the quantum photocell is defined as the chemical potential difference[15] between the two levels $|c\rangle$ and $|v\rangle$,

$$eV = e(V_c - V_v) = \mu_c - \mu_v, \tag{3}$$

Considering the Boltzmann distributions for levels $|c\rangle$ and $|v\rangle$,

$$p_c = \mathrm{e}^{-\left(\frac{E_c-\mu_c}{k_\mathrm{B}T}\right)}, \quad p_v = \mathrm{e}^{-\left(\frac{E_v-\mu_v}{k_\mathrm{B}T}\right)}, \tag{4}$$

and the voltage of the photocell can written, with respect to the energy levels and populations, as[15,24,25]

$$eV = E_c - E_v + k_\mathrm{B}T_a \ln\left(\frac{p_c}{p_v}\right). \tag{5}$$

Meanwhile, the acceptor's states $|c\rangle$ with any excess energy will radiate phonons into the ambient environment. The recombination between the acceptor and the donor is also considered with a decay rate of $\chi\Gamma$, where χ is the RRR, a dimensionless fraction. This loss channel brings the system back into the ground state without producing a work current, which could be a significant source of inefficiency. Finally, the state $|v\rangle$ decays back to the ground state $|b\rangle$, closing the cycle. In spite of another crucial loss procedure, the phonon-mediated energy relaxation still exits in this model, which are included in our kinetic model via the relaxation rates γ_1, γ_2, and $\tilde{\gamma}_1$, $\tilde{\gamma}_2$. We argue that inhibiting the radiative radiation is an efficient approach to enhance the quantum yield in our propose. In the following comments, we focus on how to control radiative radiation rate in this photocell model. Assuming that the donor molecular is directly populated by the absorption of weak incoherent solar photons ($\hbar\nu_\mathrm{s}$), the kinetics of the optically excited states obey the Lindblad master equation

$$\frac{\mathrm{d}}{\mathrm{d}t}\hat{\rho}_\mathrm{s} = -\mathrm{i}[\hat{H}, \hat{\rho}_\mathrm{s}] + \mathscr{L}\hat{\rho}_\mathrm{s}, \tag{6}$$

where $\hat{H}$ can be taken from Eq. (2), and $\mathscr{L}$ is the Lindblad super operator. Considering the two degenerated conduction bands $|a_1\rangle$, $|a_2\rangle$, the master equations in the interaction picture for Fig. 1 can be explicitly given as follows:

$$\begin{aligned}
\dot{\rho_{11}} &= -\gamma_1[(n+1)\rho_{11} - n\rho_{bb}] - \tilde{\gamma}_1[(n_c+1)\rho_{11} - n_c\rho_{cc}] \\
&\quad -\gamma_{12}(n+1)\mathrm{Re}[\rho_{12}] - \tilde{\gamma}_{12}(n_c+1)\mathrm{Re}[\rho_{12}], \\
\dot{\rho_{22}} &= -\gamma_2[(n+1)\rho_{22} - n\rho_{bb}] - \tilde{\gamma}_2[(n_c+1)\rho_{22} - n_c\rho_{cc}] \\
&\quad -\gamma_{12}(n+1)\mathrm{Re}[\rho_{12}] - \tilde{\gamma}_{12}(n_c+1)\mathrm{Re}[\rho_{12}], \\
\dot{\rho_{12}} &= -\frac{1}{2}[(\gamma_1+\gamma_2)(n+1) + (\tilde{\gamma}_1+\tilde{\gamma}_2)(n_c+1)]\rho_{12} \\
&\quad -\frac{\gamma_{12}}{2}[(n+1)\rho_{22} + (n+1)\rho_{11} - 2n\rho_{bb}] \\
&\quad -\frac{\tilde{\gamma}_{12}}{2}[(n_c+1)\rho_{22} + (n_c+1)\rho_{11} - 2n_c\rho_{cc}], \\
\dot{\rho_{cc}} &= \tilde{\gamma}_1[(n_c+1)\rho_{11} - n_c\rho_{cc}] + \tilde{\gamma}_2[(n_c+1)\rho_{22} - n_c\rho_{cc}] \\
&\quad +2\tilde{\gamma}_{12}(n_c+1)\mathrm{Re}[\rho_{12}] - \Gamma(1+\chi)\rho_{cc}, \\
\dot{\rho_{vv}} &= \Gamma\rho_{cc} - \Gamma_c(n_v+1)\rho_{vv} + \Gamma_c n_v\rho_{bb},
\end{aligned} \tag{7}$$

when the electronic system interacts with radiation and phonon thermal reservoirs, the thermal solar photons with frequency ν_s are assumed to direct onto the photocell. They drive $|a_1\rangle \leftrightarrow |b\rangle$ and $|a_2\rangle \leftrightarrow |b\rangle$ transitions with the same average occupation number $n = \frac{1}{\mathrm{e}^{(E_{a_ib}/k_\mathrm{B}T_\mathrm{s})-1}}$ and T_s is the solar temperature. The ambient thermal phonons at temperature T_a drive the two low-energy transitions $|c\rangle \leftrightarrow |a_i\rangle$ and $|v\rangle \leftrightarrow |b\rangle$. Their corresponding phonon occupation numbers are set as $n_c = \frac{1}{\mathrm{e}^{(E_{a_ic}/k_\mathrm{B}T_a)-1}}$ and $n_v = \frac{1}{\mathrm{e}^{(E_{bv}/k_\mathrm{B}T_a)-1}}$, with E_{a_ic} and E_{bv} being their corresponding energy gaps, respectively. Here $\gamma_{12} = p_1\sqrt{\gamma_1\gamma_2}$, $\tilde{\gamma}_{12} = p_2\sqrt{\tilde{\gamma}_1\tilde{\gamma}_2}$ describe the quantum coherence between the relaxation rates γ_1, γ_2, and $\tilde{\gamma}_1$, $\tilde{\gamma}_2$, respectively; p_1 and p_2 quantitatively illustrate their strengths of the quantum interference.

Considering the steady solution to Eq. (7), one can obtain the expression of the delivering power $P = j \cdot V$, to the external load circuit as a function of the RRR χ. Furthermore, utilizing the energy level populations in the steady status and

the Boltzmann distribution,[43] the expression of RRR χ can also be obtained as functions of other parameters such as the energy gaps, absorbed photon wavelength and quantum coherence generated by different relaxation channels.

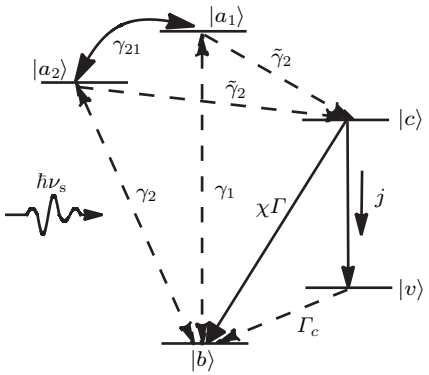


Fig. 1. Quantum photocell models consisting of two dipole-dipole coupled donors and the acceptor. Solar radiation ($\hbar\nu_s$) drives transitions between the valence band state $|b\rangle$ and the conduction band state $|a_{i,(i=1,2)}\rangle$. The curve with double arrows represent dipole-dipole coupled interaction between the conduction band state $|a_{i,(i=1,2)}\rangle$. The dashed curves represent the transferring channels of electrons. Transitions between level $|a_i\rangle_{i=1,2} \leftrightarrow |c\rangle$, $|v\rangle \leftrightarrow |b\rangle$ are connected to a load.

3. Results and discussion

It is know that the losses due to radiative recombination in principle represent one of major loss mechanisms.[15] Therefore, based on Fig. 1, we propose a parametric toy solar cell model to explore the effect of radiative recombination on the charge transport process, and study its influence on the quantum yields.

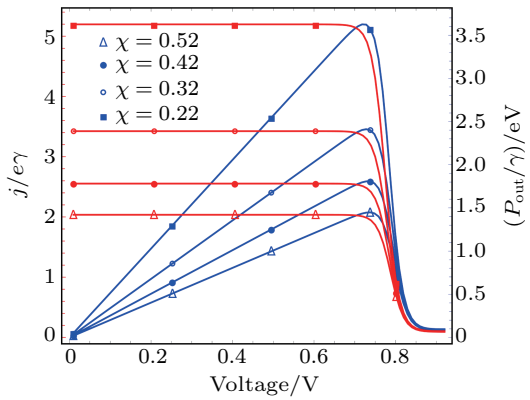


Fig. 2. Current j and power P_{out} as a function of induced cell voltage V with different RRR χ. The red and blue curves designate the output current j and delivered power P_{out}, respectively. It takes $\gamma_1 = \sqrt{2}\gamma$ eV, $\gamma_2 = 0.1\gamma_1$, $\tilde{\gamma}_1 = 50\gamma_1$, $\tilde{\gamma}_2 = 5.5\gamma_1$, $p_1 = 0.45$, $p_2 = 0.75$, $\Gamma = 1.5\gamma$, $\Gamma_c = 0.1\gamma_1$, $E_{cv} = 1.3$ eV, $E_{a_{i,(i=1,2)}b} = 1.43$ eV, $E_{a_{i,(i=1,2)}c} = E_{bv} = 0.01$ eV, $J_{12} = 0.50$ eV with γ being the scale unit.

The current–voltage characteristic (red curves) and power (blue curves) delivered to the external load circuit versus the RRR χ are plotted in Fig. 2 with their parameters shown in its caption at the room temperature $T_a = 0.0259$ eV and the solar temperature $T_s = 0.5$ eV. The results show that the peak currents and powers decrease with the increments of RRR by 0.1, and RRR's uniform increments generate the unequal reductions both for peak currents and powers. For example, the decrement of the peak values within the range from 0.22 to 0.32 of χ is larger than that within the range from 0.42 to 0.52 indicated by the red curves, and the similar characteristic is also shown by the blue curves in Fig. 2. The nonlinear influence on the quantum yields has also presented in a different quantum photocell model.[24] Figure 2 manifests the nontrivial passive role of the RRR χ in the quantum yields in this quantum photocell.

Therefore, it is of great significance to inhibit the radiative recombination in this quantum photocell model. Scully[15] proposed that the quantum yields in a different quantum photocell could be enhanced by the quantum coherence with or without driving fields compared to the classic one. In this quantum photocell, the Fano quantum coherence can be generated from two transition channels, i.e., $|a_i\rangle \leftrightarrow |b\rangle$ channel, and $|a_i\rangle \leftrightarrow |c\rangle$ channel. In the following, the RRR χ will be discussed as functions of the transition rates γ_1 and γ_2 in Fig. 3. The contour lines in Fig. 3 show the shockwave type curves, and the values for different contour lines increase with the increasing transition rates γ_1 and γ_2, which can be observed by the white numbers on the diagonal lines in Fig. 3. Meanwhile, it is also noted that transition rates γ_1 and γ_2 are different in one contour line with the same value RRR χ, and γ_1, γ_2 on the diagonal simultaneously have the smallest values. For example, among the three points A, B, and C in the contour line with RRR $\chi = 5.36\%$, the point B on the diagonal has smaller γ_1 and γ_2 (here $\gamma_1 = \gamma_2$) than those corresponding to other two points A and C.

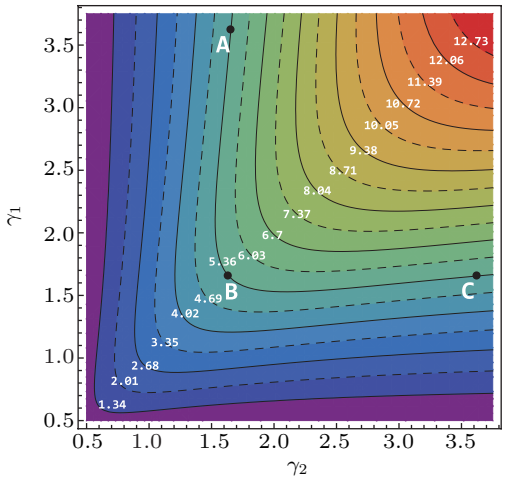


Fig. 3. Contour plot of the radiative recombination rate χ as functions of the transition rates γ_1 and γ_2. The parameters used here are $\tilde{\gamma}_1 = 3.5\gamma_2$, $\tilde{\gamma}_2 = 3.5\gamma_1$, $p_1 = p_2 = 0.80$, $\Gamma = 0.1\gamma$, $\Gamma_c = 0.45\gamma$, $E_{cv} = 0.15$ eV, $E_{a_{i,(i=1,2)}c} = E_{bv} = 0.05$ eV, and the other parameters are the same as those in Fig. 2.

In this proposed photocell model, it should be mentioned that the quantum coherence is expressed by $\gamma_{12} = p_1\sqrt{\gamma_1\gamma_2}$, $\tilde{\gamma}_{12} = p_2\sqrt{\tilde{\gamma}_1\tilde{\gamma}_2}$ with p_1, p_2 quantitatively describing their

strengths. In Fig. 3, a more robust quantum coherence, i.e., $p_1 = p_2 = 0.80$, is considered in this photocell. Hence, the inhibited RRR χ with the largest value 12.73% is achieved in Fig. 3. The increasing γ_1 and γ_2 can also influence the quantum coherence in two different transition channels, i.e., $|a_i\rangle \leftrightarrow |b\rangle$ channel and $|a_i\rangle \leftrightarrow |c\rangle$ channel, due to their parametric relations between γ_1, γ_2 and $\tilde{\gamma}_1$, $\tilde{\gamma}_2$ in Fig. 3. Here $\tilde{\gamma}_1$ and $\tilde{\gamma}_2$ indicate that the most robust quantum coherence will be achieved by the equal transition rates γ_1 and γ_2. As a result, the inhibition of the RRR χ is the most prominent, which can be manifested by three points A, B and C on the contour line with $\chi = 5.36\%$.

The quantum coherence has been proved to be a very effective way to inhibit radiative recombination in this proposed quantum photocell. Are there any other ways to inhibit radiative recombination except for the quantum coherence? In the following, Fig. 4 shows the controlled radiative recombination when the photocell system is operating under other parametric conditions with a weaker quantum interference, i.e., $p_1 = p_2 = 0.35$. The RRR χ is plotted as functions of the energy gaps $E_{a_ic} = E_{bv}$, absorbed photon wavelength λ between the levels $|a_i\rangle_{i=1,2}$ and $|b\rangle$. Considering the fact that the solar spectrum ranges from about 354 nm to 2480 nm, the absorbed photon wavelength λ falls in this range as shown in Fig. 4. Figure 4 explicitly illustrates that the RRR χ increases with the increment of gap $E_{a_ic} = E_{bv}$ when the photocell absorbs photons with a certain wavelength, while greatly increases when the photocell absorbs a longer-wavelength photon. However, the RRR χ gains far less when the gap energy $E_{a_ic} = E_{bv}$ is less than 0.2 with absorbing different-wavelength photons. In a word, the inhibited RRR χ can be achieved with a smaller energy gap ($E_{a_ic} = E_{bv}$) when it absorbs shorter-wavelength photons.

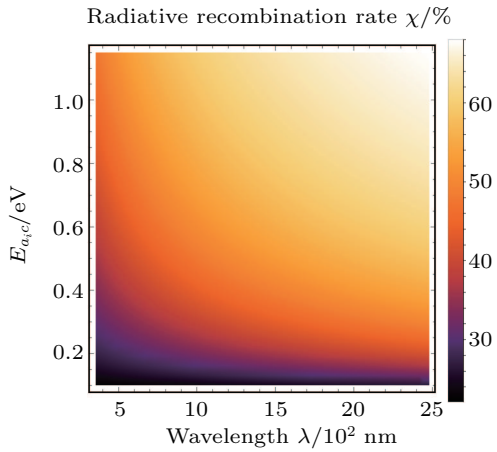


Fig. 4. Radiative recombination rate χ as functions of the energy gap E_{a_ic} and absorbed photon wavelength λ between the levels $|a_i\rangle_{i=1,2}$ and $|b\rangle$. It takes the parameters $\gamma_1 = 1.5\gamma$, $\gamma_2 = 0.5\gamma_1$, $p_1 = p_2 = 0.35$, $\Gamma_c = 4.5\gamma_1$, $E_{cv} = 1.05$ eV. The other parameters are the same as those in Fig. 3.

The physical regime reflected in Fig. 4 comes from two aspects. One is the the electron transfer process, the other is the absorbed photons. In this proposed photocell, the gaps $E_{a_ic} = E_{bv}$ designate the difficulty of electron transferring from the donor to acceptor. When the photocell with smaller gaps $E_{a_ic} = E_{bv}$, more photo-generated electrons are transferred smoothly to the acceptor and delivered to perform utilizing work, and less electrons radiate to the ground state $|b\rangle$. On the contrary, photo-generated electrons are difficult to transfer to the acceptor when the photocell system has a larger gap between the donor and acceptor, most of them radiate to the ground state $|b\rangle$, which results in the larger RRR χ. However, the higher-energy solar photon is absorbed and more energetic electrons are excited. The energetic electrons have a higher probability of transport to the acceptor, which also brings out the inhibited RRR χ.

Before concluding this work, we would like to point out some items. Although we try to use some experimental parameters to carry out theoretical discussion, we have not carried out the corresponding experimental verification. Our results may enlighten the current field of experimental research, and can even propose some interesting experimental research within this theoretical framework. We also remark that the theoretical significance will be considered in our forthcoming investigations.

4. Conclusions

In this work, we have proposed a inhibited RRR scenario in a quantum photocell with two coupled donors. After gazing at the influence of the RRR on the quantum yields, we explore the relationships among the quantum coherence generated by two different transition channels, gaps between the donor and acceptor, and the absorbed photon wavelength dependent RRR χ. The results reveal that the quantum coherence generated by the monotone increments of transition rates γ_1 and γ_2 cannot furthest inhibit the RRR, whereas the quantum coherence generated by two equal γ_1 and γ_2 has a better inhibition on the RRR, which is different from the proposal of radiative recombination reduced by the mentioned quantum coherence scheme.[15] When the energy gap between donor and acceptor is small, the transport of photo-generated electrons is more smoothly carried out, and the inhibition effect on the RRR is more robust. When the short-wavelength photons are absorbed by this photocell, more photo-generated electrons with more kinetic energy could be transported to the external load more quickly, which results in the smaller RRR. These theoretical results may enlighten the current field of experimental research, and can even be helpful for proposal of some interesting experimental research within this theoretical framework.

References

[1] Würfel P 2016 *Physics of solar cells: from basic principles to advanced concepts* 3rd edn (Birlin: Wiley-VCH)
[2] Huang H B, Tian G Y, Zhou L, Yuan J R, Fahrner W R, Zhang W B, Li X B, Chen W H and Liu R Z 2018 *Chin. Phys. B* **27** 038502
[3] Du H J, Wang W C and Gu Y F 2017 *Chin. Phys. B* **26** 028803
[4] Chen W B, Xu Z X, Li K, Chui S S Y, Roy V A L, Lai P T and Che C M 2012 *Chin. Phys. B* **21** 078401
[5] Shockley W and Queisser H J 1961 *J. Appl. Phys.* **32** 510
[6] Henry C H and Henry C H 1980 *J. Appl. Phys.* **51** 4494
[7] Li J M, Chong M, Zhu J C, Li Y J, Xu J D, Wang P D, Shang Z Q, Yang Z K, Zhu R H and Cao X L 1992 *Appl. Phys. Lett.* **60** 2240
[8] Bruns J, Seifert W, Wawer P, Winnicke H, Braunig D and Wagemann H G 1994 *Appl. Phys. Lett.* **64** 2700
[9] Luque A and Mart A 1997 *Phys. Rev. Lett.* **78** 5014
[10] Kasai H and Matsumura H 1997 *Sol. Energy Mater. Sol. Cells* **48** 93
[11] Han L Y, Koide N, Chiba Y, Islam A, Komiya R, Fuke N, Fukui A and Yamanaka R 2005 *Appl. Phys. Lett.* **86** 213501
[12] Engel G S, Calhoun T R, Read E L, Tae-Kyu A, Tomäs M, Cheng Y C, Blankenship R E and Fleming G R 2007 *Nature* **446** 782
[13] Mukti R J, Hossain M R, Islam A, Mekhilef S and Horan B 2019 *Energies* **12** 2602
[14] Guo P F, Ye Q, Yang X K, Zhang J and Wang H Q 2019 *J. Mater. Chem. A* **7** 2497
[15] Scully M O 2010 *Phys. Rev. Lett.* **104** 207701
[16] Scully M O, Chapin K R, Dorfman K E, Moochan B K and Anatoly S 2011 *Proc. Natl. Acad. Sci. USA* **108** 15097
[17] Svidzinsky A A, Dorfman K E and Scully M O 2011 *Phys. Rev. A* **84** 053818
[18] Kühn O and Lochbrunner S 2011 *Semiconductors and Semimetals* **85** 47
[19] Killoran N, Huelga S F and Plenio M B 2015 *J. Chem. Phys.* **143** 155102
[20] Yao Y 2015 *Phys. Rev. B* **91** 045421
[21] Zhang Y T, Sangchul O, Alharbi F H, Engel G S and Sabre K 2015 *Phys. Chem. Chem. Phys.* **17** 5743
[22] Sangchul O 2017 arXiv:1709.08337
[23] Daryani M, Rostami A, Darvish G and Farshi M K M 2017 *Opt. Quantum Electron.* **49** 255
[24] Zhao S C and Chen J Y 2019 *New J. Phys.* **21** 103015
[25] Zhao S C and Wu Q X 2020 *Superlattices Microstruct.* **137** 106329
[26] Handy R J 1967 *Solid State Electron.* **10** 765
[27] Sağlam M, Ayyildiz E, Gümüs A, Türüt A, Efeoğlu H and Tüzemen S 1996 *Appl. Phys. A* **62** 269
[28] Kar G S, Maikap S, Banerjee S K and Ray S K 2002 *Semicond. Sci. Technol.* **17** 938
[29] Kajiyama Y, Joseph K, Kajiyama K, Kudo S and Aziz H 2012 *Sid Symp. Dig. Tech. Papers* **43** 1544
[30] Luque A, Mellor A, Ramiro I, Antoln E, Tobas I and Mart A 2013 *Sol. Energy Mater. Sol. Cells* **115** 138
[31] Tian L and Dagenais M 2015 *Appl. Phys. Lett.* **106** 171101
[32] Kum H, Dai Y S, Aihara T, Slocum M A, Tayagaki T, Fedorenko A, Polly S J, Bittner Z, Sugaya T and Hubbard S M 2018 *Appl. Phys. Lett.* **113** 043902
[33] Richards B S 2006 *Sol. Energy Mater. Sol. Cells* **90** 2329
[34] Conibeer G, Patterson R, Huang L M, Guillemoles J F, Konig D, Shrestha S and Green M A 2010 *Sol. Energy Mater. Sol. Cells* **94** 1516
[35] Hirst L, Führer M, Farrell D J *et al.* 2011 *37th IEEE Photovoltaic Specialists Conference* (Seattle, WA) p. 003302
[36] Conibeer G, Shrestha S, Huang S J, Patterson R, Aliberti P, Xia H, Feng Y, Gupta N, Smyth S and Liao Y 2012 *38th IEEE Photovoltaic Specialists Conference* (Austin, TX) p. 000032
[37] Graziani F R 2004 *J. Quant. Spectrosc. Radiat. Transfer* **83** 711
[38] Yi Y, Massuda A, Roques-Carmes C, Kooi S E, Christensen T, Johnson S G, Joannopoulos J D, Miller O D, Kaminer I and Soljai M 2018 *Nat. Phys.* **14** 67
[39] Würfel P 2007 *CHIMIA Int. J. Chem.* **61** 770
[40] Creatore C, Parker M A, Emmott S and Chin A W 2013 *Phys. Rev. Lett.* **111** 253601
[41] Abramavicius D, Benoit P and Shaul M 2009 *Chem. Phys.* **357** 79
[42] Dorfman K E, Voronine D V, Shaul M and Scully M O 2013 *Proc. Natl. Acad. Sci. USA* **110** 2746
[43] Dorfman K E, Svidzinsky A A and Scully M O 2013 *Coherent Opt. Phenom.* **1** 42